# Journal of Materials Chemistry A



### **PAPER**

View Article Online
View Journal



Cite this: DOI: 10.1039/d5ta01128k

## Structure transformations and ionic conductivity in germanides of sodium and potassium†

Alexey P. Maltsev, \*\*D \*\*a Anastasiia V. Iosimovska, \*\*D \*\*a Ilya V. Chepkasov \*\*D \*\*a and Artem R. Oganov \*\*D \*\*a

In this study, structural transformations and ionic conductivity of sodium and potassium germanides were investigated using density functional theory and molecular dynamics simulations with machine learning interatomic potentials. Thermodynamically stable and metastable phases of Na–Ge and K–Ge systems were identified, confirming previously predicted NaGe, Na<sub>2</sub>Ge, and Na<sub>9</sub>Ge<sub>4</sub> as stable in the Na–Ge system, and K<sub>4</sub>Ge<sub>23</sub>, K<sub>3</sub>Ge<sub>17</sub>, and KGe in the K–Ge system. Thermal stability and ionic conductivity were analyzed, revealing that several metastable Na–Ge structures remain kinetically stable up to 600 K. Most Na–Ge phases have high ionic conductivity up to 10<sup>-2</sup> S cm<sup>-1</sup> at room temperature, due to low diffusion activation barriers and interconnected diffusion paths. In contrast, K–Ge phases exhibit limited structural diversity and diffusion, primarily vacancy-driven, with ionic conductivity an order of magnitude lower than Na–Ge compounds. The use of machine learning potentials allowed us to study large systems (several thousands atoms), and long (several nanoseconds) molecular dynamics runs with *ab initio* accuracy. Our findings suggest that Na–Ge and K–Ge compounds hold potential as anode materials due to their favorable ionic conductivity and stability at moderate and elevated temperatures.

Received 11th February 2025 Accepted 9th April 2025

DOI: 10.1039/d5ta01128k

rsc.li/materials-a

#### 1 Introduction

Lithium-ion batteries (LIBs) have revolutionized human life, but there is a need for new types of batteries and battery materials. Limited reserves of lithium, and its cost, necessitate the development of batteries based on alternative active ions. Replacing the graphite anode (which has a theoretical capacity

"Skolkovo Institute of Science and Technology, Bolshoy Boulevard 30, bld. 1, Moscow, 121205, Russian Federation. E-mail: alexey.maltsev@skoltech.ru; a.oganov@skoltech.ru

<sup>b</sup>Katanov Khakas State University, 90 Lenin pr., 655017 Abakan, Russia

† Electronic supplementary information (ESI) available: Table S1: energy and force errors on the training set for Na-Ge and K-Ge MLIP. Table S2: comparison between experimental and calculated using DFT and MTP-MLIP lattice parameters in NaGe and KGe structures. Fig. S1: scheme of machine-learning interatomic potential construction procedure. Fig. S2: energy errors on the validation data set and their distribution for the Na-Ge MLIP. Fig. S3: force errors on the validation data set and their distribution for the Na-Ge MLIP. Fig. S4: energy errors on the validation data set and their distribution for the K-Ge MLIP. Fig. S5: force errors on the validation data set and their distribution for the K-Ge MLIP. Fig. S6: snapshots of the Na<sub>13</sub>Ge<sub>4</sub> and Na<sub>19</sub>Ge<sub>2</sub> structures, obtained at different time steps and temperatures. Fig. S7: sodium diffusion trajectories in stable and metastable Na-Ge compounds. Fig. S8: stable and metastable structures in the K-Ge system and their space groups. Fig. S9: binary convex hull for K-Ge system, and ionic conductivity in conductive K-Ge phases. Fig. S10: charge difference (cross-section through 110 plane) for a different NaGe and KGe phases. Machine learning interatomic potentials for Na-Ge and K-Ge systems, their training sets. POSCARS for stable metastable Na-Ge and K-Ge structures. DOI: https://doi.org/10.1039/d5ta01128k

of 372 mA h g<sup>-1</sup>) with other materials possessing higher energy density may increase the overall energy density of a battery. Such materials are also needed for sodium and potassium ion batteries, which could be cheaper than LIBs.<sup>3</sup> Sodium and potassium are promising candidates for battery applications also due to their low electrochemical potential, abundance, and non-toxicity. However, only a small number of devices have been commercialized to date, such as ZEBRA-type and sodiumsulfur batteries,<sup>4-6</sup> which typically operate at high temperatures or in stationary applications.<sup>5</sup>

Various anode materials have been proposed for metal-ion batteries, including alloys,7 composites,8 and organic elec-Phosphides,11,12 silicides,13,14 germanides,16-18 and metal-based alloys,7 are superior to other types of anodes due to their extremely high specific capacity, which can exceed thousands of mA h g-1. However, despite their high capacity, these materials suffer from significant volume changes during charge-discharge processes, which can exceed several hundred percent, leading to interface instability, device cracking, dendrite growth, and, consequently, short circuits, explosions, and other safety issues. 19 Nevertheless, it is possible to overcome these disadvantages by creating composite or hierarchical structures. For instance, phosphorus incorporated inside single-walled nanotubes has recently been tested as an anode material for LIBs.20,21 The design of composite current collectors and adjustments to the anode microstructure may also improve cyclability; for example, germanium anodes with a composite current collector made of  ${
m Co_3O_4}$  nanorods can maintain a high capacity of more than 1000 mA h  ${
m g^{-1}}$  after 600 charge–discharge cycles. 16

Germanium anode is considered promising due to its high specific capacity (1564 mA h g<sup>-1</sup> in Li<sub>17</sub>Ge<sub>4</sub>, 830 mA h g<sup>-1</sup> in Na<sub>9</sub>Ge<sub>4</sub>, and 369 mA h g<sup>-1</sup> in KGe), which is higher or comparable with other anodes for Na/K-ion batteries, for instance, 125 mA h g<sup>-1</sup> in graphite, up to 900 mA h g<sup>-1</sup> in graphite modifications and composites, 22 240 mA h g<sup>-1</sup> in TiO<sub>2</sub>, 23 510 mA h  $g^{-1}$  in  $Mo_2S_3$ , <sup>23</sup> 409 mA h  $g^{-1}$  in Amorphous  $FeO_x$ , <sup>23</sup> 615 mA h g<sup>-1</sup> in amorphous MoS<sub>3</sub>,<sup>23</sup> etc. Other advantages of germanium are high electronic17 and ionic conductivities18,24 of compounds, and good surface stability.25 Various thermodynamic and kinetic properties of Li-Ge phases have been investigated both experimentally and theoretically. For instance, many phases have been predicted to be thermodynamically stable or metastable through density functional theory (DFT) calculations. 13,18,26 Many of these phases, including metastable ones, have been obtained experimentally during electrochemical processes.27 The ionic conductivity of stable and lowlying metastable Li-Ge phases was previously studied by us18 using molecular dynamics (MD) and machine learning interatomic potentials (MLIP). It was shown that most of these phases exhibit high ionic conductivity of approximately 10<sup>-2</sup> S cm<sup>-1</sup> at room temperature, with the diffusion topology depending on the lithium concentration within the structure.

Sodium and, especially, potassium germanides have been studied to a lesser extent. Recently, Darby *et al.*<sup>28</sup> utilized DFT, MLIP, and *ab initio* random structure searching (AIRSS)<sup>29</sup> to predict stable Na–Ge compounds at pressures of 0 and 10 GPa. Jung *et al.*<sup>30</sup> employed DFT calculations and *ab initio* molecular dynamics (AIMD) to investigate amorphous Ge as an anode material for sodium-ion batteries, showing high ionic conductivity in amorphous Na–Ge phases. Li *et al.*<sup>31</sup> conducted DFT calculations to support experimental studies on complex Ge–P–C anodes for sodium-ion batteries, demonstrating that the activation barriers for Na diffusion in such anodes are less than 300 meV. Loaiza *et al.*<sup>32</sup> provided a comprehensive report on alloyed Si- and Ge-anodes for lithium, sodium, and potassium, while also noting the limited number of reports available to date.

The ionic conductivity in crystalline Na-Ge and K-Ge phases remains unstudied. In this work, we employ DFT calculations and MD simulations, utilizing MLIP, to investigate the thermodynamic and kinetic properties of sodium and potassium germanides. Our study focuses on: phase transformations concerning metal concentration; diffusion of Na and K in thermodynamically stable and low-lying metastable structures; and thermally induced structural transformations.

## 2 Computational methods

All DFT calculations were performed using the VASP code  $^{33-36}$  with the PAW method  $^{37,38}$  and the optB88-vdW functional.  $^{39,40}$  This functional was used in our previous calculations  $^{18}$  of Li–Ge binary compounds, and we retained all the methods to facilitate comparison between the related systems. A plane-wave energy cutoff of 400 eV and  $\Gamma$ -centered k-meshes with a reciprocal

space resolution of 0.2 Å<sup>-1</sup> were employed. We utilized the USPEX evolutionary crystal structure prediction method<sup>41-43</sup> to identify stable and metastable binary compounds. In addition to the evolutionary structure search, we considered all known compounds from the Materials Project,<sup>44</sup> OQMD<sup>45,46</sup> databases, previous works on Li–Ge and Na–Ge phases,<sup>13,28</sup> as well as related structures of alkali metal alloys with elements such as silicon, phosphorus, germanium, and tin, where the metals were replaced by sodium or potassium, and the second element was germanium.

Thermodynamic stability was assessed by the convex hull diagrams. Phases located on the convex hull are stable with respect to decomposition into elemental structures or other binary compounds. The convex hull is constructed geometrically on a diagram of the Gibbs formation energy *versus* composition. The Gibbs formation energy is defined as

$$\Delta G(\mathbf{M}_x \mathbf{G} \mathbf{e}_y) = \frac{G(\mathbf{M}_x \mathbf{G} \mathbf{e}_y) - xG(\mathbf{M}) - yG(\mathbf{G} \mathbf{e})}{(x+y)}, \tag{1}$$

where M is either Na or K. Gibbs free energy of formation includes the zero point energy correction, and entropy contribution, which were calculated using harmonic approximation within the phonopy package.<sup>47</sup> Dynamic stability of all considered stable and metastable structures was proved by the absence of imaginary frequencies. Symmetry of the structures was analyzed using spglib python package<sup>48</sup> with 0.02 tolerance factor. Ge–Ge bond orders were estimated using integrated crystal orbital bond index approach (iCOBI),<sup>49</sup> implemented in the LOBSTER<sup>50,51</sup> code. Charge transfer from sodium and potassium atoms to germanium atoms was evaluated as a difference between the integrated electron densities of the structure and isolated cations/anions.

Molecular dynamics were performed using LAMMPS code52,53 and Moment Tensor machine learning potential (MTP)<sup>54,55</sup> of 20-th level. MTP potential was trained on binary and single-element compounds. The initial data set for the interatomic potential was collected from AIMD trajectories. Active learning (AL) approach 56 was used to improve the quality of the MLIP. The scheme of AL is shown on Fig. S1 of ESI.† Final training sets consist of 1136 and 1236 structures for Na-Ge and K-Ge systems. Where possible, we used supercell structures in training, such that the lattice parameters exceeded 10 Å. Root mean square errors (RMSE) of energies and forces after the training are 9 meV per atom and 143 meV Å<sup>-1</sup> for Na-Ge system. In K-Ge system RMSE of energy is 8 meV per atom and RMSE of forces is 91 meV Å<sup>-1</sup>. Further validation of MLIPs also indicate the quality of the constructed potentials (see Fig. S2-5, and Tables S1 and S2 in the ESI†).

Thermal stability of the structures was assessed using MD simulations of annealing, during which the structures were: (a) heated from 1 K to 600 K with the heating rate of  $10^{11}$  K s<sup>-1</sup>, (b) equilibrated at 600 K for 0.5 ns, (c) cooled down to 0 K at the same rate as were heating, and (d) reoptimized at 0 K. Diffusion coefficients and ionic conductivities were calculated at 300, 350, 400, 450 and 500 K, after the preliminar equilibration at the target temperature for 1 ns. Each simulation in LAMMPS was

performed with NPT ensemble and Nose-Hoover thermostat<sup>57,58</sup> with a 1 fs timestep. Supercell structures were constructed in such way that the lattice parameters exceeded 30 Å, such structures typically have from 1000 to 3000 atoms. 1% vacancies at metallic sites were added to include the vacancy diffusion mechanism into consideration. Both techniques for thermal stability and diffusion calculations, as well as MLIP construction procedure, were tested by us before, and it was shown that the methodology gives the reasonable results in good agreement with experiments.<sup>59</sup> Diffusion coefficients were calculated using mean square displacements (MSD) of cations:

$$D = \frac{1}{6} \lim_{t \to \infty} \frac{\mathrm{d}}{\mathrm{d}t} \frac{1}{N} \sum_{i=1}^{N} \left\langle \left| r_i(t) - r_i(0) \right|^2 \right\rangle \tag{2}$$

where N – is number of mobile atoms in the supercell, i – atomic number of mobile ion,  $r_i(0)$ ,  $r_i(t)$  – radius vectors from the host center of mass to the *i*th atom at time 0 and *t*, respectively.

Ionic conductivities were calculated using the Nernst-Einstein formula:

$$\sigma = \frac{nq^2D}{H_{\rm r}k_{\rm B}T}\tag{3}$$

where n is the mobile ion density, q is the formal charge of the ion (q = 1),  $k_B$  is Boltzmann constant, T is temperature and  $H_r$  is Haven ratio (assumed to be 1).

Activation energy Ea of diffusion was calculated using the Arrhenius formula:

$$D = D_0 \times \exp\left(\frac{-E_a}{k_B T}\right) \tag{4}$$

#### Results and discussion

Fig. 1 shows the calculated convex hull for the binary Na-Ge system. Our calculations indicate that only three binary compounds are thermodynamically stable at room temperature: NaGe  $(I4_1/acd)$ , Na<sub>2</sub>Ge  $(R\bar{3}m)$ , and Na<sub>9</sub>Ge<sub>4</sub> (R3m). This result is consistent with previous studies,28 with one exception:

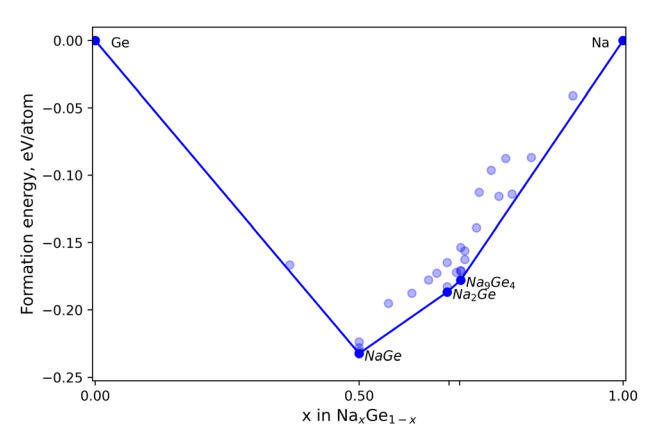


Fig. 1 Calculated convex hull of the Na–Ge system at T = 300 K. Filled blue circles and transparent circles represent stable and metastable compounds, respectively.

our calculations predict that the most stable geometry of Na<sub>9</sub>Ge<sub>4</sub> possesses R3m symmetry, rather than the  $P\bar{1}$  symmetry reported by Darby et al.28 Notably, the R3m structure was not identified by USPEX, instead, the C2/m structure was predicted, however imaginary frequencies were observed in the phonon band-structures, indicating dynamical instability. A crystal structure with displacements along the q-points associated with the imaginary modes was created and re-optimized, resulting in the identification of a stable structure with R3m symmetry. Furthermore, the P1 structure of Na<sub>9</sub>Ge<sub>4</sub> also exhibited dynamical instability in our calculations, even though the authors of the authors of paper28 fixed the imaginary modes of the same C2/m structure.<sup>28</sup> It is seen that the potential energy surface in sodium-germanium system might be very sensitive to the used computational approach, including the choice of the DFT functional.

There are many metastable structures, for the NaGe, Na<sub>2</sub>Ge, Na<sub>9</sub>Ge<sub>4</sub> compositions, as well as for other compositions. Table 1 shows their chemical formulas, energies above the convex hull, and space groups. Some of these structures have previously been presented in the databases, either directly as Na-Ge compounds or as related AM-X compounds (where AM = Li, Na, K, and X = Si, Ge).

Fig. 2 shows stable and low-lying metastable Na-Ge structures. These structures might be divided in several groups based

Table 1 List of stable and metastable structures of Na-Ge system. Thermodynamically stable compounds are highlighted in bold

Composition	$E_{\rm hull}$ , meV per atom	Space group (no.)	Origin
Ge	0	$Fd\bar{3}m~(227)$	MP-database (ref. 44)
Na <sub>7</sub> Ge <sub>12</sub>	5	$P\bar{1}$ (2)	Li <sub>7</sub> Ge <sub>12</sub> (ref. 18)
NaGe	0	I4 <sub>1</sub> /acd (142)	LiGe (ref. 44)
NaGe	3	$P2_{1}/c$ (14)	MP-database (ref. 44)
NaGe	9	$P\bar{4}3n$ (218)	KGe (ref. 44)
NaGe	9	C2/c (15)	KGe (ref. 46)
Na <sub>5</sub> Ge <sub>4</sub>	22	Pbam (55)	Ref. 28
Na <sub>3</sub> Ge <sub>2</sub>	21	$P6_3mc$ (186)	Ref. 28
Na <sub>12</sub> Ge <sub>7</sub>	17	$Pna2_{1}(33)$	Li <sub>12</sub> Ge <sub>7</sub> (ref. 44)
Na <sub>11</sub> Ge <sub>6</sub>	17	$Cmc2_1$ (36)	Li <sub>11</sub> Ge <sub>6</sub> (ref. 44)
Na <sub>2</sub> Ge	0	C2/m~(12)	Ref. 28
Na <sub>2</sub> Ge	0.4	$R\bar{3}m$ (166)	Li <sub>2</sub> Si (ref. 44)
Na <sub>2</sub> Ge	19	C2/m(12)	USPEX
Na <sub>13</sub> Ge <sub>6</sub>	7	C2/m(12)	Li <sub>13</sub> Ge <sub>6</sub> (ref. 18)
Na <sub>9</sub> Ge <sub>4</sub>	0	R3m (160)	USPEX
Na <sub>9</sub> Ge <sub>4</sub>	9	$P2_{1}(4)$	USPEX
Na <sub>9</sub> Ge <sub>4</sub>	22	$R\bar{3}m$ (166)	USPEX
Na <sub>9</sub> Ge <sub>4</sub>	12	$P6_3/mmc$ (194)	Li <sub>9</sub> Ge <sub>4</sub> (ref. 44)
Na <sub>7</sub> Ge <sub>3</sub>	11	$P2_{1}(4)$	USPEX
Na <sub>7</sub> Ge <sub>3</sub>	17	$P\bar{3}m1$ (164)	USPEX
Na <sub>13</sub> Ge <sub>5</sub>	18	$P\bar{3}m1(164)$	Li <sub>13</sub> Si <sub>5</sub> (ref. 44)
Na <sub>8</sub> Ge <sub>3</sub>	48	P1 (1)	Ref. 28
Na₃Ge	50	Pnma (62)	Ref. 28
Na <sub>13</sub> Ge <sub>4</sub>	17	Pm (6)	Li <sub>13</sub> Ge <sub>4</sub> (ref. 18)
Na <sub>7</sub> Ge <sub>2</sub>	46	P2/m (10)	Ref. 28
Na <sub>15</sub> Ge <sub>4</sub>	5	$I\bar{4}3d$ (220)	Li <sub>15</sub> Ge <sub>4</sub> (ref. 44)
Na <sub>19</sub> Ge <sub>4</sub>	15	$I\bar{4}2m(121)$	USPEX
Na <sub>19</sub> Ge <sub>2</sub>	17	$P\bar{1}$ (2)	USPEX
Na	0	$Im\overline{3}m$ (229)	MP-database (ref. 44)

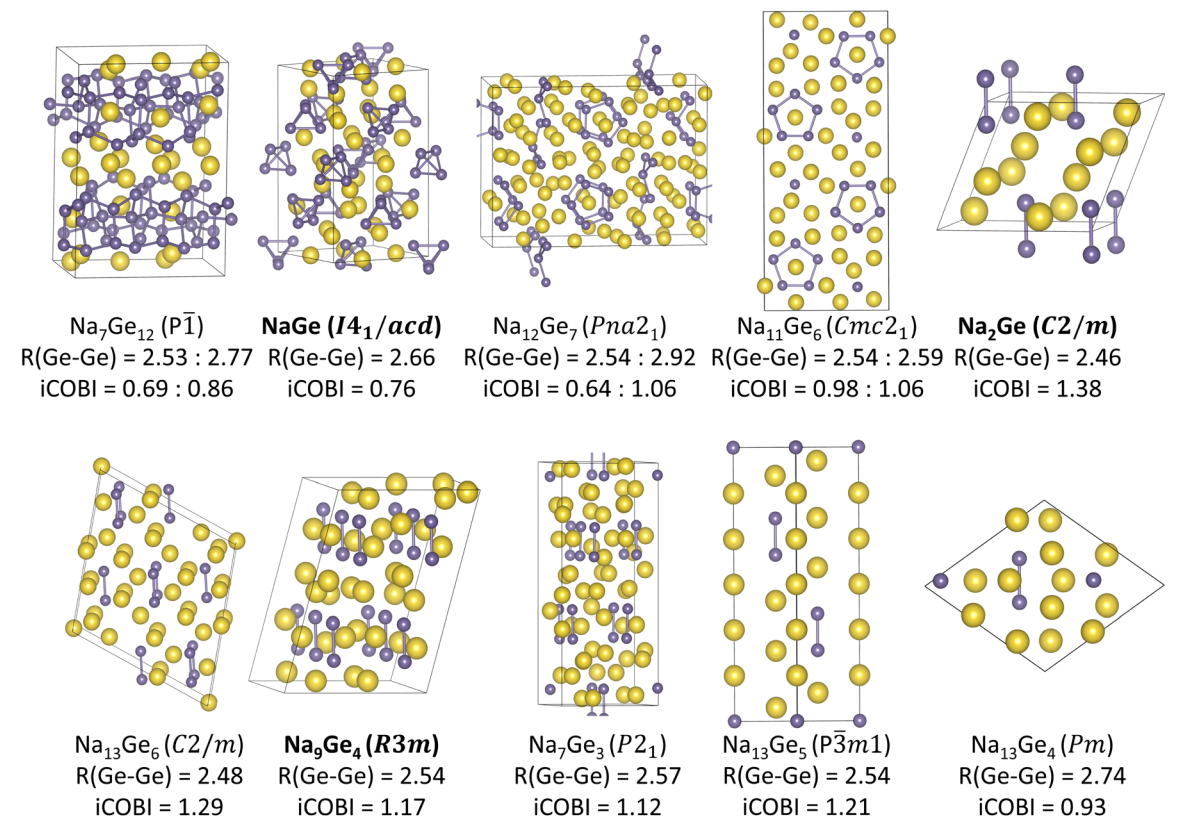


Fig. 2 Stable and metastable structures in the Na-Ge system, their space groups, Ge-Ge bond lengths, and iCOBI. Thermodynamically stable compounds are highlighted in bold.

on the sodium to germanium ratio and the Ge-arrangement in the structure, which obeys the Zintl-Klemm concept and 8 - Nrule: pristine germanium has 4 valence electrons, and thus, 4 covalent bonds. If alkali metals donate one electron to germanium, such as when N(Na)/N(Ge) = 1, then germanium has 5 electrons and only 3 covalent bonds. If N(Na)/N(Ge) = 2, then germanium has 6 electrons, and is expected to have two covalent bonds; if N(Na)/N(Ge) = 3, the germanium is expected to have only one covalent bond; and if N(Na)/N(Ge) = 4, germanium is expected to be isolated from other Ge atoms.

The only one compound with N(Na)/N(Ge) ratio less than 1 is Na<sub>7</sub>Ge<sub>12</sub>. Only seven of the twelve germanium atoms accept electrons from sodium and have three covalent bonds; the remaining five germanium atoms have four covalent bonds, forming a tetrahedral environment with other germanium atoms. In NaGe, Ge atoms form  $\mathrm{Ge_4}^{4-}$  tetrahedra, the stable structure and its metastable isomorphs differ only by slightly different arrangement of Na cations.

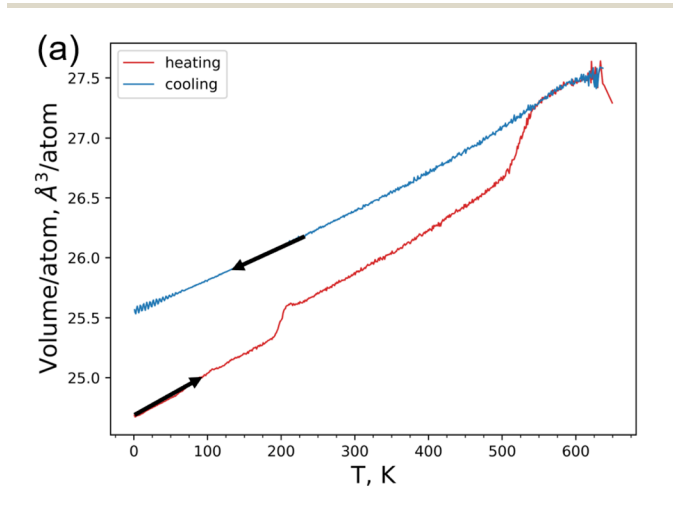
 $Na_{12}Ge_7$  and  $Na_{11}Ge_6$  are intermediate structures with  $1 \le$  $N(\text{Na})/N(\text{Ge}) \le 2$ . In these structures, 5-membered Ge rings are formed, in which each Ge atom has two covalent bonds. The remaining Ge atoms either form umbrella-shaped structures or are isolated, and deviating from the 8 - N rule, and thus, are likely to be subject to substitution, doping or defect formation.

In compounds with  $2 \le N(Na)/N(Ge) \le 3$  (Na<sub>2</sub>Ge, Na<sub>13</sub>Ge<sub>6</sub>, Na<sub>9</sub>Ge<sub>4</sub>, Na<sub>7</sub>Ge<sub>3</sub>, Na<sub>13</sub>Ge<sub>5</sub>) germanium atoms form 2-atom Ge-Ge dumbbells, which, at first glance, deviate from the 8 - N

rule. However, calculations indicate that these dumbbells have shortened bonds (~2.46-2.54 Å), compared to compounds in which single bonds between germanium atoms are observed (2.66 Å in NaGe and 2.92 Å in Na<sub>12</sub>Ge<sub>7</sub>). At the same time, calculated iCOBI values, which denote the Mayer bond orders, range from 1.12 to 1.38 (for comparison, in NaGe this value is 0.76). These facts may indicate a multiple bond character for Ge-Ge bonds in the dumbbells, and thus, the 8 - N rule is preserved. As the concentration of sodium in the space surrounding the Ge-Ge dumbbells increases, the Ge-Ge bond gradually weakens; in the  $Na_{13}Ge_4$  (for which the N(Na) to N(Ge)ratio is already greater than 3), the distance between Ge is 2.74 Å, and the iCOBI is less than 1, indicating that the Ge-Ge in the dumbbell is a single bond. The structures mentioned above have very similar structural motifs not only due to the presence of germanium dumbbells, but also due to their mutual arrangement and alternation with sodium layers. Some of these metastable structures may be expected in experiments, and their formation may be kinetically driven during the sodiation process, as well as because of possible stabilization due to configurational entropy, partial occupancy of individual positions, non-stoichiometric compounds with defects.

Ge-Ge bond eventually breaks in the Na<sub>15</sub>Ge<sub>4</sub> structure (in which N(Na)/N(Ge) is close to 4), and all configurations with higher Na concentrations have isolated Ge atoms.

To evaluate the thermal stability of the structures with  $E_{\text{hull}}$  < 20 meV per atom, we performed MD simulations involving heating and annealing at 600 K, followed by cooling to 0 K. The 20 meV per atom threshold is supported by prior research indicating that many observed metastable compounds typically exhibit small energy differences from the ground state, with a median value around 15 meV per atom, suggesting that this value enhances the likelihood of synthesizability while maintaining computational efficiency.60 Na7Ge12, NaGe, Na11Ge6, Na<sub>2</sub>Ge, Na<sub>13</sub>Ge<sub>6</sub>, Na<sub>9</sub>Ge<sub>4</sub>, Na<sub>7</sub>Ge<sub>3</sub>, and Na<sub>15</sub>Ge<sub>4</sub> are thermally stable up to 600 K, exhibiting no phase transitions or disordering. Na<sub>12</sub>Ge<sub>7</sub>, and Na<sub>13</sub>Ge<sub>5</sub> are also stable, but there are phase transitions from ordered to disordered structures. Fig. 3 shows an example of volume as a function of temperature for the Na<sub>13</sub>Ge<sub>5</sub> structure during heating-cooling simulations, and partial radial distribution functions before and after annealing. At temperatures above 500 K, even at the absence of vacancies, sodium ions exhibit high self-diffusion and occupy different positions surrounding the Ge-sublattice; these order-disorder transformations are not reversible, and partial occupancy remains in the structures after cooling and re-optimization. Disordered structures of Na<sub>12</sub>Ge<sub>7</sub> and Na<sub>13</sub>Ge<sub>5</sub> have increased



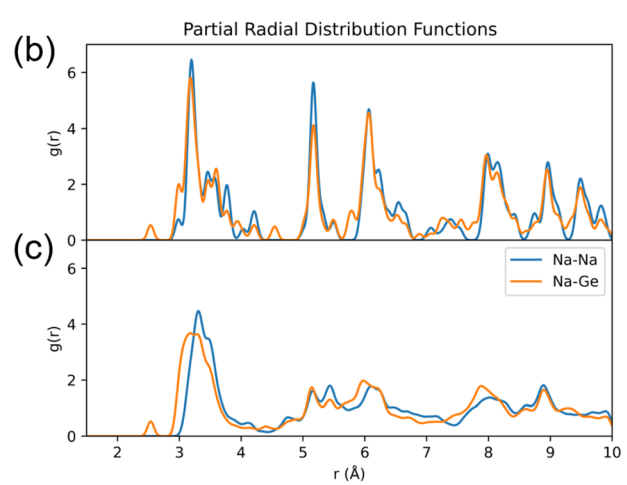


Fig. 3 Volume as a function of temperature for Na<sub>13</sub>Ge<sub>5</sub> during heating and cooling simulations (a), and partial radial distribution functions corresponding to Na-Na and Na-Ge bonds before annealing (b) and after (c)

volumes by 2.8% and 3.2%, respectively. At the same time, disordered structures exhibit small gain in the energy of 9 meV per atom and 18 meV per atom (with the respect to the ordered structures) according to calculations with the MTP MLIP. During the MD simulations,  $Na_{13}Ge_4$  melts at T > 400 K, and does not crystallize back, remaining in the amorphous phase, at least under the simulation conditions. High sodium concentration compounds Na<sub>19</sub>Ge<sub>4</sub> and Na<sub>19</sub>Ge<sub>2</sub> are thermally unstable and decompose at temperatures above 300 K into a metallic sodium phase and amorphous binary Na-Ge phases. Thus, Na<sub>13</sub>Ge<sub>4</sub>, Na<sub>19</sub>Ge<sub>4</sub>, and Na<sub>19</sub>Ge<sub>2</sub> are not expected to be synthesized. Snapshots of the Na<sub>13</sub>Ge<sub>4</sub> and Na<sub>19</sub>Ge<sub>2</sub> structures, obtained at different time steps and temperatures, are provided in Fig. S6† (ESI) to illustrate their phase transitions.

Molecular dynamics simulations allowed us to compute ionic conductivity and diffusion pathways in the stable Na-Ge phases. Fig. S7 of the ESI† shows the calculated diffusion trajectories in the Na-Ge compounds. Diffusion trajectories depend on the Ge motifs. For instance, the Na<sub>7</sub>Ge<sub>12</sub> compound, in which two-dimensional spatially connected structures of Ge atoms are formed, has two-dimensional diffusion channels located between the Ge layers. Diffusion in Na<sub>12</sub>Ge<sub>7</sub> and Na<sub>11</sub>Ge<sub>6</sub> also occurs predominantly in planes perpendicular to the 5-membered rings; however these diffusion channels are connected, and overall diffusion is three-dimensional. All compounds with  $2 \le N(\text{Li})/N(\text{Ge}) \le 3$  exhibit a threedimensional diffusion, which, however, occurs predominantly in planes perpendicular to the Ge-Ge dumbbells. Na<sub>15</sub>Ge<sub>4</sub>, as well as NaGe, have three-dimensional diffusion, since all the Geions or Ge44- tetrahedra, respectively, are surrounded by Naions. Notably, all the compounds, except NaGe, have connected trajectory pathways, even in simulations without vacancies, indicating high self-diffusion and a cooperative mechanism of diffusion in these structures. In the absence of vacancies, NaGe is the only compound in which there are no connections between the trajectory lines, even at an increased temperature of 600 K, indicating that the diffusion mechanism is exceptionally vacancy-based. Na7Ge12 unit cell has 2 unique sodium layers, one of which shows self-diffusion, and diffusion in the second occurs only through vacancy jumps.

Fig. 4 shows the ionic conductivity of stable and metastable Na-Ge compounds as a function of temperature. The lowest ionic conductivity values are for the Na<sub>7</sub>Ge<sub>12</sub> and NaGe phases, in which diffusion is limited by the presence of vacancies. It should be noted that values of  $\sim 10^{-3}$  S cm<sup>-1</sup> at room temperatures are overestimated because realistic vacancy concentrations should be much lower than the 1% used in the simulations. Other compounds show high ionic conductivity of  $\sim 10^{-2}$  -  $10^{-1}$  S cm<sup>-1</sup> even at room temperatures, and low diffusion activation energies. Higher ionic radius of sodium atom, compared to that of lithium, results in decrease of ionic conductivity by approximately an order of magnitude, in comparison with related Li-Ge system. 18

In contrast to the Na-Ge system, the K-Ge binary system is represented by only a few compounds. There are only three thermodynamically stable phases: K<sub>3</sub>Ge<sub>17</sub> (Fd3m), K<sub>4</sub>Ge<sub>23</sub> (P4<sub>2</sub>/ mmc) and KGe  $(P\overline{4}3n)$ . The KGe composition has three

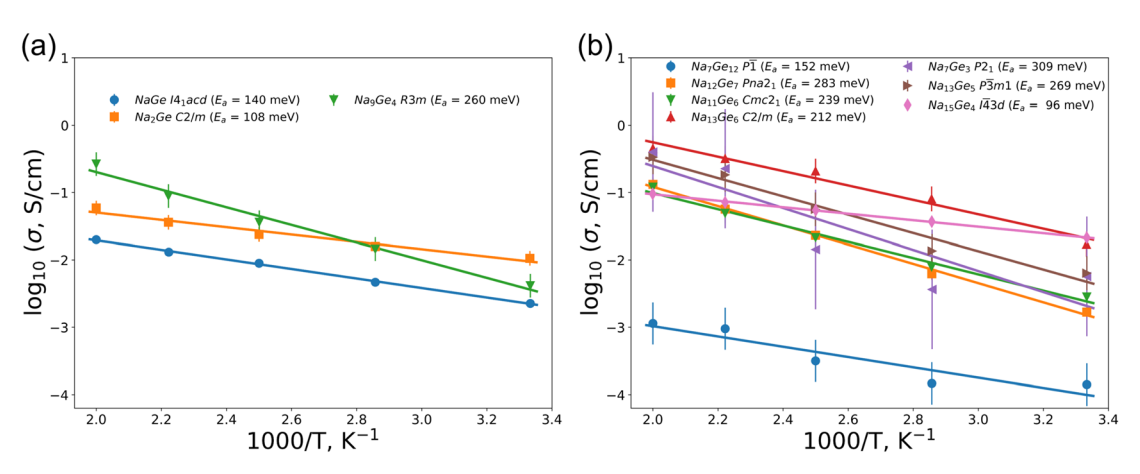


Fig. 4 Ionic conductivity of stable (a) and metastable (b) Na-Ge binary compounds.

metastable isomorphs:  $I4_1/acd$ , C2/c, and  $P\overline{1}$ , which are 2 meV per atom, 5 meV per atom, and 9 meV per atom above the convex hull, respectively. The only metastable structure, K<sub>5</sub>Ge<sub>4</sub>  $(P\bar{1})$ , is 16 meV per atom above the convex hull. Stable and metastable structures are shown in Fig. S8 of the ESI.† Fig. S9a of the ESI† shows convex-hull for the binary K-Ge system. According to the molecular dynamics, all these phases are thermodynamically stable, and no phase transitions or disordering was found. K<sub>4</sub>Ge<sub>23</sub> and K<sub>3</sub>Ge<sub>17</sub> form host-guest structures, in which Ge atoms form three-dimensional wireframe structures, and potassium atoms are located in the spaces inside. As a result, there are no connected diffusion channels in the structures, and no diffusion is observed. Unlike most Na-Ge phases, KGe and K<sub>5</sub>Ge<sub>4</sub> do not show potassium self-diffusion without vacancies even at elevated temperatures above 500 K. Vacancy induces diffusion in KGe and K5Ge4 is lower than in Na-Ge compounds by approximately an order of magnitude, and is about  $10^{-4}$ – $10^{-3}$  S cm<sup>-1</sup> at room temperature. Ionic conductivity as a function of temperature is shown in Fig. S9b of the ESI.† The observed reduction in ionic conductivity, when compared to sodium-based phases, may be attributed to the enhanced bonding interactions between the metal ions and germanium atoms, as evidenced by charge density difference maps. These maps, calculated for representative NaGe and KGe phases (see Fig. S10 of the ESI†), reveal a more pronounced charge accumulation in the interstitial region between potassium and germanium, indicative of stronger covalent character in K-Ge bonds. This trend aligns with prior observations in bilayer alkali metal structures, further supporting the correlation between increased charge transfer and bond strength in potassium-containing systems.61

#### 4 Conclusions

To conclude, in this work we have comprehensively studied the Na–Ge and the K–Ge binary systems. Using density functional theory calculations and the USPEX evolutionary algorithm, we have constructed convex hulls, representing all thermodynamically stable and low-lying metastable structures. The USPEX

method allowed us to find many new Na-Ge phases for the first time.

In the Na–Ge system, there are three thermodynamically stable phases: NaGe, Na<sub>2</sub>Ge, and Na<sub>9</sub>Ge<sub>4</sub>. Many metastable structures with  $E_{\rm hull}$  less than 20 meV per atom were found, and their properties were analyzed. Using molecular dynamics and machine learning interatomic potentials (moment tensor potentials), we have studied their thermal stability and ionic conductivity. Low-energy metastable compounds Na<sub>7</sub>Ge<sub>12</sub>, Na<sub>11</sub>Ge<sub>6</sub>, Na<sub>13</sub>Ge<sub>6</sub>, Na<sub>7</sub>Ge<sub>3</sub>, and Na<sub>15</sub>Ge<sub>4</sub> are dynamically stable and it may be possible to obtain them experimentally. All the structures have high ionic conductivity at room temperature (from  $\sim 10^{-3}$  to  $\sim 10^{-2}$  S cm<sup>-1</sup>) and low activation barriers of diffusion not exceeding 350 meV. Diffusion paths form connected 3D or 2D trajectories even in the absence of vacancies, for all compounds except NaGe, for which the mechanism of diffusion is entirely vacancy-based.

Structural and chemical diversity in the K–Ge system is much less than in the Na–Ge system. We have found three phases to be thermodynamically stable:  $K_4Ge_{23}$ ,  $K_3Ge_{17}$ , and KGe, but only one low-energy metastable compound  $K_5Ge_4$ . All these phases are kinetically stable at elevated temperatures up to 600 K.  $K_4Ge_{23}$  and  $K_3Ge_{17}$  have a guest–host structures, in which there are no connected diffusion channels of potassium, and therefore, no diffusion in them was observed. Diffusion in KGe and  $K_5Ge_4$  is an order of magnitude lower than in the related Na–Ge compounds.

We have shown that there are many stable and low-energy metastable Na–Ge and K–Ge compounds, most of which have exceptionally high ionic conductivities, comparable to those of related Li–Ge compounds, despite much larger ionic radii of Na and K. Our findings suggest that germanium is a promising anode material for sodium-ion batteries.

## Data availability

The data supporting this article have been included as part of the ESI,† including MTP machine learning interatomic potentials for the Na-Ge and K-Ge systems, their training and validation data sets, as well as all crystal structures in VASP format (POSCAR).

#### **Author contributions**

Paper

Alexey P. Maltsev: conceptualization; methodology; formal analysis; investigation; writing – original draft; visualization. Anastasiia V. Iosimovska: investigation. Ilya V. Chepkasov: conceptualization; methodology; Artem R. Oganov: supervision; writing – review & editing.

#### Conflicts of interest

There are no conflicts to declare.

## Acknowledgements

The study was supported by the Russian Science Foundation. All calculations were supported by Grant No. 19-72-30043. The calculations were carried out using the resources of the Center for the Information and Computing of the Research Center for Information and Computational Technologies at Novosibirsk State University and the Arkuda supercomputers at Skoltech.

#### References

- 1 J. B. Goodenough and Y. Kim, *Chem. Mater.*, 2010, 22, 587-603.
- 2 J.-J. Kim, K. Yoon, I. Park and K. Kang, Small Methods, 2017, 1, 1700219.
- 3 K. Kubota, M. Dahbi, T. Hosaka, S. Kumakura and S. Komaba, *Chem. Rec.*, 2018, **18**, 459–479.
- 4 Y. Zhao, K. R. Adair and X. Sun, *Energy Environ. Sci.*, 2018, **11**, 2673–2695.
- 5 B. L. Ellis and L. F. Nazar, Curr. Opin. Solid State Mater. Sci., 2012, 16, 168–177.
- 6 H. Pan, Y.-S. Hu and L. Chen, Energy Environ. Sci., 2013, 6, 2338–2360.
- 7 X. Gu, J. Dong and C. Lai, Eng. Rep., 2021, 3, e12339.
- 8 P. Shi, X.-Q. Zhang, X. Shen, R. Zhang, H. Liu and Q. Zhang, *Adv. Mater. Technol.*, 2020, 5, 1900806.
- 9 A. V. Desai, R. E. Morris and A. R. Armstrong, *ChemSusChem*, 2020, 13, 4866–4884.
- 10 A. P. Maltsev, I. V. Chepkasov and A. R. Oganov, *Mater. Today Energy*, 2024, **39**, 101467.
- 11 A. P. Maltsev, I. V. Chepkasov, A. G. Kvashnin and A. R. Oganov, *Crystals*, 2023, 13, 756.
- 12 M. Mayo, K. J. Griffith, C. J. Pickard and A. J. Morris, *Chem. Mater.*, 2016, **28**, 2011–2021.
- 13 A. J. Morris, C. Grey and C. J. Pickard, *Phys. Rev. B:Condens. Matter Mater. Phys.*, 2014, **90**, 054111.
- 14 L. Lin, X. Xu, C. Chu, M. K. Majeed and J. Yang, *Angew. Chem.*, 2016, **128**, 14269–14272.
- 15 A. R. Kamali and D. J. Fray, *Rev. Adv. Mater. Sci.*, 2011, 27, 14-
- 16 X. Li, Z. Yang, Y. Fu, L. Qiao, D. Li, H. Yue and D. He, *ACS Nano*, 2015, **9**, 1858–1867.

- 17 X. Liu, X.-Y. Wu, B. Chang and K.-X. Wang, *Energy Storage Mater.*, 2020, **30**, 146–169.
- 18 A. V. Iosimovska, A. P. Maltsev, I. V. Chepkasov and A. R. Oganov, Appl. Phys. Lett., 2024, 124, 163904.
- 19 C. Yang, K. Fu, Y. Zhang, E. Hitz and L. Hu, Adv. Mater., 2017, 29, 1701169.
- 20 D. Rybkovskiy, V. Koroteev, A. Impellizzeri, A. Vorfolomeeva, E. Y. Gerasimov, A. Okotrub, A. Chuvilin, L. Bulusheva and C. Ewels, *ACS Nano*, 2022, 16, 6002–6012.
- 21 A. A. Vorfolomeeva, S. G. Stolyarova, I. P. Asanov, E. V. Shlyakhova, P. E. Plyusnin, E. A. Maksimovskiy, E. Y. Gerasimov, A. L. Chuvilin, A. V. Okotrub and L. G. Bulusheva, *Nanomaterials*, 2022, 13, 153.
- 22 Y. Dou, L. Zhao, Y. Liu, Z. Zhang, Y. Zhang, R. Li, X. Liu, Y. Zhou, J. Wang and J. Wang, *Carbon Neutralization*, 2024, 3, 954–995.
- 23 Y. Wan, B. Huang, W. Liu, D. Chao, Y. Wang and W. Li, *Adv. Mater.*, 2024, **36**, 2404574.
- 24 C. Fuller and J. Severiens, Phys. Rev., 1954, 96, 21.
- 25 W. Liang, H. Yang, F. Fan, Y. Liu, X. H. Liu, J. Y. Huang,T. Zhu and S. Zhang, ACS Nano, 2013, 7, 3427–3433.
- 26 W. W. Tipton, C. A. Matulis and R. G. Hennig, *Comput. Mater. Sci.*, 2014, **93**, 133–136.
- 27 H. Jung, P. K. Allan, Y.-Y. Hu, O. J. Borkiewicz, X.-L. Wang, W.-Q. Han, L.-S. Du, C. J. Pickard, P. J. Chupas, K. W. Chapman, et al., Chem. Mater., 2015, 27, 1031–1041.
- 28 J. P. Darby, A. F. Harper, J. R. Nelson and A. J. Morris, *Phys. Rev. Mater.*, 2024, 8, 105002.
- 29 C. J. Pickard and R. Needs, J. Phys.: Condens. Matter, 2011, 23, 053201.
- 30 S. C. Jung, H.-J. Kim, Y.-J. Kang and Y.-K. Han, *J. Alloys Compd.*, 2016, **688**, 158–163.
- 31 W. Li, X. Li, J. Liao, B. Zhao, L. Zhang, Y. Liu, L. Huang, Y. Li and M. Liu, *Energy Storage Mater.*, 2019, **20**, 380–387.
- 32 L. C. Loaiza, L. Monconduit and V. Seznec, *Small*, 2020, **16**, 1905260.
- 33 G. Kresse and J. Furthmüller, *Phys. Rev. B:Condens. Matter Mater. Phys.*, 1996, **54**, 11169.
- 34 G. Kresse and J. Furthmüller, *Comput. Mater. Sci.*, 1996, 6, 15–50.
- 35 G. Kresse and J. Hafner, *Phys. Rev. B:Condens. Matter Mater. Phys.*, 1993, 47, 558.
- 36 J. Hafner, Comput. Phys. Commun., 2007, 177, 6-13.
- 37 P. E. Blöchl, *Phys. Rev. B:Condens. Matter Mater. Phys.*, 1994, **50**, 17953.
- 38 G. Kresse and D. Joubert, *Phys. Rev. B:Condens. Matter Mater. Phys.*, 1999, **59**, 1758.
- 39 J. Klimeš, D. R. Bowler and A. Michaelides, *J. Phys.: Condens. Matter*, 2009, **22**, 022201.
- 40 J. Klimeš, D. R. Bowler and A. Michaelides, *Phys. Rev. B:Condens. Matter Mater. Phys.*, 2011, **83**, 195131.
- 41 A. R. Oganov and C. W. Glass, J. Chem. Phys., 2006, 124, 244704.
- 42 A. R. Oganov, A. O. Lyakhov and M. Valle, *Acc. Chem. Res.*, 2011, 44, 227–237.
- 43 A. O. Lyakhov, A. R. Oganov, H. T. Stokes and Q. Zhu, *Comput. Phys. Commun.*, 2013, **184**, 1172–1182.

- 44 A. Jain, S. P. Ong, G. Hautier, W. Chen, W. D. Richards, S. Dacek, S. Cholia, D. Gunter, D. Skinner, G. Ceder, et al., APL Mater., 2013, 1, 011002.
- 45 J. E. Saal, S. Kirklin, M. Aykol, B. Meredig and C. Wolverton, *IOM*, 2013, **65**, 1501–1509.
- 46 S. Kirklin, J. E. Saal, B. Meredig, A. Thompson, J. W. Doak, M. Aykol, S. Rühl and C. Wolverton, *npj Comput. Mater.*, 2015, 1, 1–15.
- 47 A. Togo and I. Tanaka, Scr. Mater., 2015, 108, 1-5.
- 48 A. Togo, K. Shinohara and I. Tanaka, *arXiv*, 2018, preprint, arXiv:1808.01590, DOI: 10.48550/arXiv.1808.01590.
- 49 P. C. Müller, C. Ertural, J. Hempelmann and R. Dronskowski, *J. Phys. Chem. C*, 2021, **125**, 7959–7970.
- 50 S. Maintz, V. L. Deringer, A. L. Tchougréeff and R. Dronskowski, *LOBSTER: A Tool to Extract Chemical Bonding from Plane-Wave Based DFT*, 2016.
- 51 R. Nelson, C. Ertural, J. George, V. L. Deringer, G. Hautier and R. Dronskowski, *J. Comput. Chem.*, 2020, 41, 1931–1940.
- 52 S. Plimpton, J. Comput. Phys., 1995, 117, 1-19.

- 53 A. P. Thompson, H. M. Aktulga, R. Berger, D. S. Bolintineanu, W. M. Brown, P. S. Crozier, P. J. in't Veld, A. Kohlmeyer, S. G. Moore, T. D. Nguyen, et al., Comput. Phys. Commun., 2022, 271, 108171.
- 54 A. V. Shapeev, Multiscale Model. Simul., 2016, 14, 1153-1173.
- 55 I. S. Novikov, K. Gubaev, E. V. Podryabinkin and A. V. Shapeev, *Mach. Learn.: Sci. Technol.*, 2020, 2, 025002.
- 56 E. V. Podryabinkin, E. V. Tikhonov, A. V. Shapeev and A. R. Oganov, *Phys. Rev. B*, 2019, **99**, 064114.
- 57 W. G. Hoover, Phys. Rev. A, 1986, 34, 2499.
- 58 D. J. Evans and B. L. Holian, *J. Chem. Phys.*, 1985, **83**, 4069–4074.
- 59 A. P. Maltsev, I. V. Chepkasov and A. R. Oganov, ACS Appl. Mater. Interfaces, 2023, 15, 42511–42519.
- 60 W. Sun, S. T. Dacek, S. P. Ong, G. Hautier, A. Jain, W. D. Richards, A. C. Gamst, K. A. Persson and G. Ceder, Sci. Adv., 2016, 2, e1600225.
- 61 I. V. Chepkasov, M. Ghorbani-Asl, Z. I. Popov, J. H. Smet and A. V. Krasheninnikov, *Nano Energy*, 2020, 75, 104927.